EuroSun2026

IMPACT OF THERMAL ABSORBER DESIGN ON THE PERFORMANCE AND MANUFACTURING VIABILITY OF PVT COLLECTORS

Muhammad Talha Jahangir[1], Abel Climente García[1], Ivan Acosta-Pazmiño[1,2 *]
[1]MG Sustainable Engineering AB, 753 21 Uppsala, Sweden
[2]Department of Building Engineering, University of Gävle, 801 76 Gävle, Sweden
[*] ivan@mgsust.com

Summary

This work investigates the role of thermal absorber design in flat-plate and low-concentrating photovoltaic–thermal (PVT) collectors using a Computational Fluid Dynamics (CFD) based assessment approach. Three absorber configurations were analyzed for each collector type and compared with the reference design, with the results validated against experimental data to evaluate thermal efficiency, heat-loss behavior, and hydraulic performance. Flat-plate PVT collectors targeting heat pump integration benefit from absorber designs that enhance heat dissipation, resulting in improved system thermal efficiency and a higher collector heat-loss coefficient: the zero-loss efficiency rises from 0.486 to 0.525 and the heat loss coefficient from 19.3 to 24.3 W/(m²·K), while the pressure loss falls by up to 80%. For low-concentrating PVT collectors intended for low- to medium-industrial applications, absorber geometry primarily influences heat-loss reduction and zero-loss thermal efficiency, and only the micro-grooved design lowers the heat loss coefficient, by 5.0%, at the cost of a 120.8% higher pressure loss. An optimized cost-based analysis of manufacturing processes comparing vacuum forming and extrusion routes highlights a production volume threshold, approximately 7,200 units for the flat-plate absorber and 14,800 units for the low-concentrating absorber, at which extrusion becomes economically favorable. The results demonstrate the importance of application-specific absorber design and manufacturing-aware optimization. Experimental validation within the PVT4EU project and extended analyses of electrical, economic, and environmental aspects are planned for future journal publication.

Flat Plate Collectors (FPCs), Concentrating Photovoltaic thermal collectors (CPVTs)

Field of application for the findings: Heat pump integration (FPCs) & High temperature applications (CPVTs)

Addressed audience: PVT researchers, system designers, and manufacturers involved in PVTs.

1. Introduction

Photovoltaic–thermal (PVT) collectors deliver electricity and useful heat from the same aperture area, which makes them attractive where roof space is limited and both energy carriers are needed (Herrando et al., 2023). Their useful operating range covers two application domains with growing demand in Europe: low-temperature heat supply as a source for heat pumps in buildings, and low- to medium-temperature process heat for industry. Which collector concept suits which domain depends strongly on how the design balances heat extraction against thermal losses at the intended operating temperature (Lämmle et al., 2017).

The thermal absorber is a key component of PVT collectors, as it governs heat extraction, overall efficiency, and the practical feasibility of system deployment (Kurniawati and Sung, 2024). This is because absorber design also directly affects manufacturability and production cost, making it a critical factor in scaling PVT technologies across different applications. A wide range of absorber concepts has been analyzed in the literature, including sheet-and-tube, box-channel, roll-bond, and finned geometries, with CFD commonly used to compare candidate designs before prototyping (Kurniawati and Sung, 2024; Herrando et al., 2023). Beltrán et al. (2025) compared heat-exchanger designs intended specifically for heat pump integration on a techno-economic basis.

The design targets differ between the two applications. A PVT collector serving as a heat pump source frequently operates at or below ambient temperature, so a high heat-loss coefficient becomes an advantage: the absorber then gains heat from the surrounding air in addition to solar irradiance, under certain conditions (Bertram et al., 2012; Lämmle et al., 2017). Field measurements confirm that unglazed, uninsulated and finned PVT collectors can act as the sole source of a heat pump, even at ambient temperatures down to −10 °C (Beltrán et al., 2024). For industrial process heat, the priority reverses since the thermal losses should be minimized to achieve higher temperatures. Low-concentrating collectors based on compound parabolic concentrator (CPC) optics can reach temperatures up to 140 °C without tracking, but only if thermal losses from the receiver are kept low (Pranesh et al., 2019; Ramezani et al., 2024).

Polymeric absorbers are attractive for both applications owing to their low weight, corrosion resistance, and relatively low material cost, and they are compatible with high-volume production processes such as extrusion and vacuum forming (Olivares et al., 2008). The manufacturing route, in turn, constrains the channel geometries that can actually be produced: extrusion yields continuous multi-channel profiles at a high initial tooling cost, while vacuum forming allows more geometric freedom with a lower initial investment. Despite this coupling between geometry, performance, and cost, manufacturing-aware design considerations, including production processes and cost implications, are rarely integrated into performance-oriented PVT studies (Ramezani et al., 2024). In addition, comparative studies differentiating flat-plate and low-concentrating PVT absorber designs across application domains remain limited.

This study evaluates the role of thermal absorber design in determining the theoretical performance and manufacturing viability of thermal absorbers for PVT collectors across different application domains using a CFD model-based assessment approach. Two representative collector categories were considered (see Fig. 1): a flat-plate PVT collector (PVT-SP) targeting heat pump integration, and a low-concentrating PVT collector (PVT-MG) intended for low- to medium-temperature industrial applications. For the flat-plate configuration, a polymer double-plate absorber based on ABS/polycarbonate was used as the reference geometry. For the low-concentrating configuration, a reference collector employing a CPC and a bifacial receiver was considered. In both cases, different channel geometries were evaluated to assess their impact on heat-extraction effectiveness under application-relevant thermal loads. In addition, the two production routes relevant for these absorbers, vacuum forming and extrusion, were compared using a cost model to identify the production volume at which each route becomes economically preferable. The developed CFD tool and both reference designs are experimentally validated within the PVT4EU project (PVT4EU, 2026).

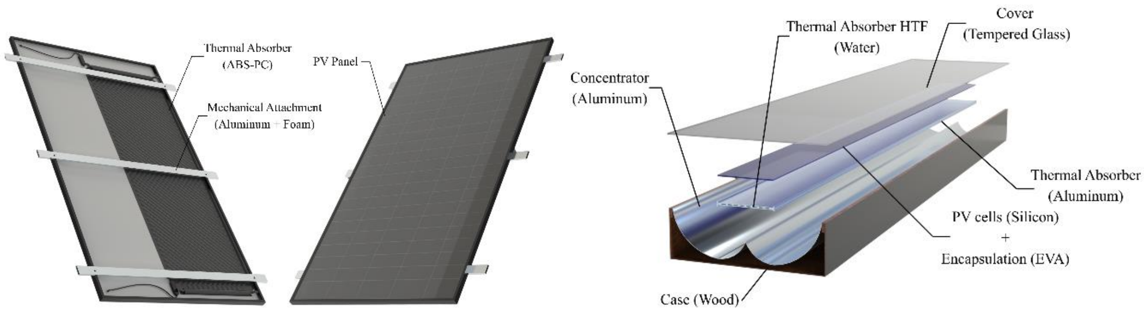

Fig. 1: Conceptual schematic representation of the investigated PVT collector concepts and their main components. Left: flat-plate PVT collector (PVT-SP). Right: low-concentrating PVT collector (PVT-MG).

The remainder of the paper is organized as follows: Section 2 describes the CFD models, the performance indicators, the boundary conditions, and the manufacturing cost model; Section 3 presents the thermal, hydraulic, and cost results; Section 4 summarizes the conclusions and outlines future work.

2. Methodology

A CFD modeling approach was implemented in COMSOL Multiphysics to assess the technoeconomic influence of thermal absorber design on the flat-plate and low-concentrating PVT collectors. For each collector type, three alternative channel configurations were evaluated and compared against the validated reference design (see Fig. 2). Configuration names reflect the intended manufacturing process: EXT denotes extrusion-based channel designs while VAC denotes vacuum-formed geometries.

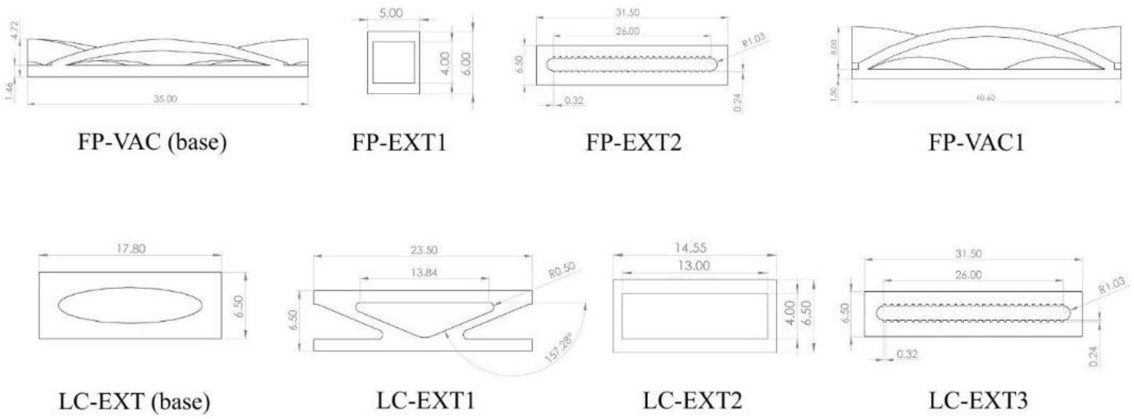

Fig. 2: Cross-sectional geometries of the investigated thermal absorber channel configurations for flat-plate (FP) and low-concentrating (LC) PVT collectors. The top row shows the flat-plate configurations, including the reference vacuum-formed design (FP-VAC) and the modified extrusion-based (FP-EXT1, FP-EXT2) and vacuum-formed (FP-VAC1) designs. The bottom row presents the low-concentrating PVT absorber configurations, including the reference extrusion-based design (LC-EXT) and the modified extrusion-based designs (LC-EXT1, LC-EXT2, LC-EXT3) considered in this study.

2.1. Reference collector designs

The flat-plate collector (PVT-SP) is a retrofit concept in which a conventional PV laminate, consisting of a glass cover, an encapsulant (EVA) layer, silicon PV cells, a second EVA layer, and a Tedlar backsheet, is attached to the polymer double-plate thermal absorber through a mechanical attaching medium. The reference absorber is vacuum-formed with an absorber area of 0.91 m², and the collector targets heat pump integration with operating temperatures between approximately −10 °C and 40 °C. The low-concentrating collector (PVT-MG) combines a compound parabolic concentrator with a bifacial receiver inside a wooden casing. The receiver stack consists of a tempered glass cover, an enclosed air volume, and a hybrid absorber in which PV cells are laminated on both faces of the absorber plate between EVA encapsulant layers (glass – air – EVA – PV cells – EVA – absorber – EVA – PV cells – EVA – air – concentrator). The reference absorber (PVT-MG-V1) is an extruded aluminium profile with inlet and outlet manifolds soldered to the absorber, and the collector targets delivery temperatures up to 140 °C. The thermophysical properties of the component materials used in both CFD models are listed in Tab. 1.

Tab. 1: Thermophysical properties of the collector component materials used in the CFD models.

Collector	Component	Material	Thermal conductivity [W/(m·K)]	Density [kg/m³]	Specific heat [J/(kg·K)]	Reference
PVT-SP	Absorber plate	ABS	0.17	1050	1470	NETZSCH (n.d.)
	PV layer	Silicon	130	2329	700	Herrando et al. (2019)
	Glass cover	Tempered glass	1.40	2210	730	
	EVA layers	EVA	0.35	960	2090	
	Backsheet	Tedlar	0.36	1250	1200	
PVT-MG	Absorber plate	Aluminium	237	2702	903	
	PV layers	Silicon	130	2329	700	
	Glass cover	Tempered glass	1.40	2210	730	
	EVA layers	EVA	0.35	960	2090	

2.2. Flat-plate collector model

For the flat-plate collector, three-dimensional steady-state simulations with laminar flow and conjugate heat transfer were performed, using a channel approach, as suggested in the literature (Beltrán et al., 2024). The absorber, the PV laminate and the fluid domain were solved as a single conjugate problem, so that the heat generated in the cells is conducted through the encapsulant layers into the absorber and removed by the working fluid. The photovoltaic electrical performance was assumed to be temperature dependent, based on the power loss coefficient of c-Si solar cells.

2.3. Low-concentrating collector model

The low-concentrating collector was modelled in two steps. The enclosed air volumes between the hybrid absorber and the tempered glass govern the internal convective losses of the receiver, and resolving the buoyancy-driven flow directly inside a full three-dimensional model would be computationally expensive; the convective behaviour was therefore characterised separately and then transferred to the three-dimensional model.

In the first step, two-dimensional simulations of the receiver cavity were performed in COMSOL Multiphysics. The convective heat transfer coefficients were first estimated using the correlation of Hollands et al. (1976) for natural convection in enclosed air layers, which provided the initial values and a reference for the simulated results. The two-dimensional model then resolved the buoyancy-driven vortices in the cavity and returned the convective coefficients from the local heat flux and the temperature difference between the absorber wall and the tempered glass (eq. 1):

$$h_{conv}\ [\mathrm{W\ m^{-2}\ K^{-1}}] = q \,/\, (T_{wall} - T_{glass}) \qquad \text{(eq. 1)}$$

where h_{conv} is the convective heat transfer coefficient in W m^{-2} K^{-1}, q is the local convective heat flux across the air layer in W m^{-2}, T_{wall} is the temperature of the absorber wall and T_{glass} is the temperature of the inner surface of the tempered glass cover, both in K.

The coefficients obtained in this way are reported in Section 3.2. In the second step, three-dimensional steady-state simulations of the full receiver were performed. The convective coefficients from the first step were imposed on the cavity boundaries, the irradiance distributions obtained from the ray-tracing simulations were applied to the absorber surfaces (Section 2.5), and conjugate heat transfer between the working fluid, the absorber and the laminated PV layers was solved together with the temperature-dependent electrical performance of the cells.

2.4. Performance indicators

Three indicators are used throughout this work to compare the absorber configurations, and each carries a different physical meaning for the application. The thermal performance of every configuration is expressed through the specific thermal power output and the instantaneous thermal efficiency (eq. 2 and eq. 3):

$$P_{th}\ [\mathrm{W/m^2}] = (\dot{m}_f \cdot c_p \cdot \Delta T) \,/\, A_c \qquad \text{(eq. 2)}$$

$$\eta_{th} = P_{th} \,/\, G \qquad \text{(eq. 3)}$$

where P_{th} is the specific thermal power output in W/m^2, $\dot{m}_f$ is the mass flow rate of the working fluid through the absorber in kg/s, c_p is the specific heat capacity of the working fluid in J/(kg·K), ΔT is the temperature rise of the fluid between the inlet and the outlet in K, A_c is the collector aperture area in m^2, η_{th} is the instantaneous thermal efficiency and G is the irradiance on the collector aperture in W/m^2.

The third indicator is the hydraulic penalty of the geometry. The pressure loss across the absorber was evaluated at the end of each steady-state simulation as the difference between the area-averaged static pressure over the inlet boundary and over the outlet boundary of the fluid domain (eq. 4):

$$\Delta p\ [\mathrm{Pa}] = p_{in} - p_{out} \qquad \text{(eq. 4)}$$

where p_{in} and p_{out} are the area-averaged static pressures over the inlet and outlet surfaces of the absorber, respectively, evaluated at the same mass flow rate for all configurations so that the geometries can be compared directly. The pressure loss determines the parasitic pumping power required to circulate the working fluid, and therefore the electricity consumed by the collector loop.

2.4. Boundary conditions

Following ISO 9806, the efficiency curve is plotted against the reduced temperature (Tm − Ta)/G and characterised by two parameters. The zero-loss efficiency η0 is the intercept of the curve and expresses how much of the incident irradiance is converted into useful heat when the absorber operates at ambient temperature, so it measures how effectively the absorber geometry removes heat from the receiver. The heat loss coefficient a1 is the slope of the curve and expresses how quickly that performance decays as the fluid temperature rises above ambient, so it measures the thermal coupling between the absorber and its surroundings. The interpretation of a1 depends on the application: for an industrial collector operating far above ambient a low value is desirable, whereas for a collector feeding a heat pump evaporator near or below ambient a high value is an advantage, because the same coupling then works in the opposite direction and allows the absorber to draw heat from the surrounding air.

Standard testing conditions were adopted to enable comparative evaluation. For the flat-plate collector, simulations were conducted at an irradiance of 800 W/m², an ambient temperature of 25 °C, and a wind speed of 1.3 m/s. For the low-concentrating collector, the irradiance distribution on the bifacial receiver was obtained from ray-tracing simulations of the concentrator performed within the PVT4EU project (PVT4EU, 2026). The resulting flux maps, with average irradiances of 865 W/m² on the top face and 1028.3 W/m² on the bottom (concentrator-facing) face of the hybrid absorber, were applied directly to the absorber surfaces (Fig. 3). Ambient and wind conditions were kept consistent with the flat-plate case, and fluid inlet temperatures were varied from 30 °C to 90 °C to cover the intended operating range.

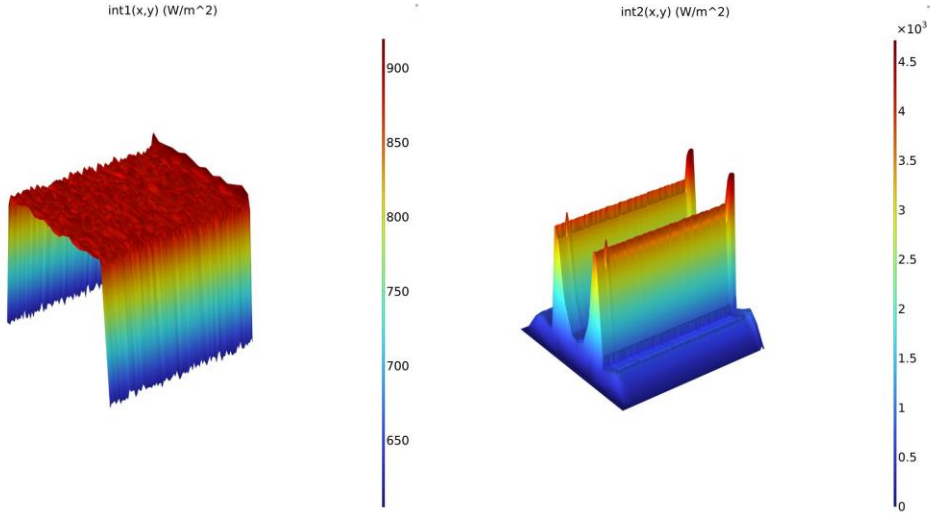

Fig. 3: Irradiance distribution applied to the hybrid absorber of the low-concentrating collector, obtained from ray-tracing simulations within the PVT4EU project. Left: flux on the top face of the thermal absorber. Right: flux on the bottom, concentrator-facing face.

2.5. Mesh independence and Model Validation

A mesh independence study was performed to determine the number of elements required for the simulations. For the flat-plate model, seven meshes between 1.14 and 7.56 million elements were compared on the basis of the predicted thermal output and the associated computation time, and the mesh was considered independent once a further refinement changed the predicted output by less than 0.1%. The same sizing criteria, expressed as the element size relative to the channel hydraulic diameter and the number of elements across the fluid layer, were then applied to the low-concentrating model, so that both models resolve the near-wall gradients to the same standard. The outcome of the study is reported in Section 3.1.

Both reference models were validated against thermal efficiency curves measured on the corresponding prototypes within the PVT4EU project. The validation compares the simulated and measured efficiency over the same range of reduced temperature, and the agreement is assessed through the zero-loss efficiency, the heat loss coefficient and the maximum deviation between the two curves. Only after this agreement was confirmed were the reference models used as the baseline against which the modified absorber geometries were evaluated; the comparison is presented in Section 3.1.

2.6. Manufacturing cost model

A manufacturing cost comparison was performed for the two production routes relevant to the investigated absorbers, vacuum forming and extrusion, using cost parameters provided by Opido (vacuum forming) and Inaventa (extrusion). A linear cost model C(x) was used (eq. 5), where x is the number of absorbers produced, m the unitary manufacturing cost and n the initial tooling investment (CAPEX). The unitary cost combines the material, labour and energy costs scaled by the absorber area (eq. 6). The break-even production volume between the two routes follows from equating the two cost functions (eq. 7):

$C(x) = m \cdot x + n$ (eq. 5)

$$m = (c_{mat} + c_{lab} + c_{en}) \cdot A_{abs} \qquad \text{(eq. 6)}$$

$$x_{be} = (n_{EXT} - n_{VAC}) / (m_{VAC} - m_{EXT}) \qquad \text{(eq. 7)}$$

where c_{mat}, c_{lab} and c_{en} are the material, labour and energy costs per unit area in €/m^2, A_{abs} is the absorber area in m^2, and the subscripts VAC and EXT denote vacuum forming and extrusion. The input parameters are listed in Tab. 2.

The analysis rests on the following assumptions. The cost of an absorber is linear in the production volume, so the unitary cost is independent of the number of units produced and no learning effects or volume discounts are included. The tooling investment is a single up-front cost that is not discounted over time, and the same tooling cost is assumed for both absorbers within a given production route. Only the thermal absorber is costed; the PV laminate, the glazing, the casing, assembly and transport are excluded, since they are common to the configurations being compared. For the low-concentrating collector, the analysis assumes a polymer variant of the absorber geometry, so that both production routes can be compared on the same basis as for the flat-plate absorber. Material, labour and energy costs were provided by manufacturers for each route and are treated as constant over the volume range considered.

Tab. 2: Input parameters of the manufacturing cost model for vacuum forming and extrusion of the flat-plate (PVT-SP) and low-concentrating (PVT-MG) absorbers.

Parameter	PVT-SP Vacuum forming	PVT-SP Extrusion	PVT-MG Vacuum forming	PVT-MG Extrusion
Material cost [€/m²]	30.00	32.73	30.00	32.73
Labour cost [€/m²]	21.18	3.18	21.18	3.18
Energy cost [€/m²]	0.88	0.21	0.44	0.10
Absorber area [m²]	0.91	0.91	0.45	0.45

3. Results

This section first reports the mesh independence study and the validation of the two reference models (Section 3.1) and the convective coefficients obtained from the two-dimensional cavity model of the low-concentrating receiver (Section 3.2). The simulated performance of the modified absorber geometries is then examined relative to the validated reference designs, first for the flat-plate collector targeting heat pump integration (Section 3.3) and then for the low-concentrating collector aimed at industrial process heat (Section 3.4). Section 3.5 links both sets of results to the manufacturing cost analysis.

3.1. Mesh independence and model validation

The mesh independence study for the flat-plate model is shown in Fig. 4. The predicted thermal output stabilizes above approximately 2.7 million elements: the deviation between the selected mesh of 3.0 million elements and the finest mesh of 7.56 million elements is 0.03%, while the computation time increases from 29 minutes to more than 2 hours. The 3.0-million-element mesh was therefore used for all flat-plate simulations. Applying the same sizing criteria to the low-concentrating model gave an equivalent result, with the predicted thermal output changing by less than 0.1% under further refinement, so the two models resolve the flow field to the same standard.

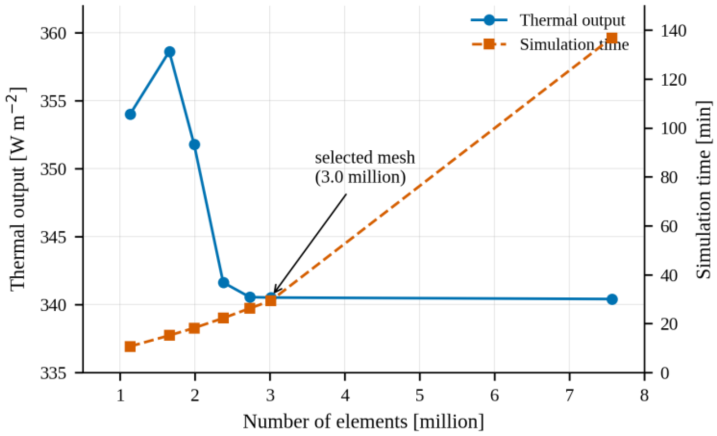

Fig. 4: Mesh independence study for the flat-plate PVT model: predicted thermal output and simulation time as a function of the number of mesh elements.

The validation of both reference models against the measured efficiency curves is presented in Fig. 5. For the flat-plate collector, the numerical model slightly underestimates the measured efficiency, with a maximum deviation below 2 percentage points of thermal efficiency across the tested range. For the low-concentrating collector, the model slightly overestimates the zero-loss efficiency (0.538 versus 0.521), while the heat loss coefficient agrees within 0.2% (5.12 versus 5.11 W m−2 K−1); the deviation remains below 1.7 percentage points over the reduced-temperature range. The validated reference models were subsequently used as the baseline for the absorber design variations.

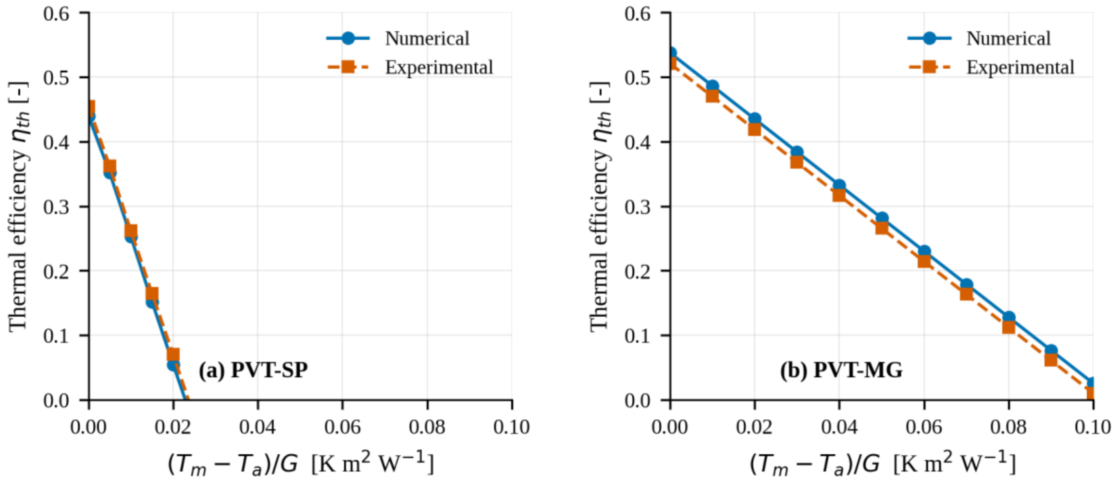

Fig. 5: Validation of the CFD models against experimental thermal efficiency curves: (a) flat-plate collector PVT-SP; (b) low-concentrating collector PVT-MG.

3.2. Internal convection in the low-concentrating receiver

Fig. 6a shows the velocity magnitude of the air flow inside the collector cavity at a receiver temperature of 75 °C. The temperature difference between the heated receiver and the cooler glass and reflector surfaces drives a natural convection flow: recirculating vortices form in the narrow gap above the receiver, a slower circulation follows the reflector wing, and the lower part of the cavity remains nearly stagnant, with air velocities of the order of 0.1 m/s. The convective exchange is therefore concentrated around the receiver. The heat transfer coefficients extracted from these simulations are shown in Fig. 6b for fluid inlet temperatures between 30 °C and 90 °C. As the buoyancy-driven flow intensifies with temperature, the convective coefficient increases from 2.20 to 3.35 W m−2 K−1 on the absorber side and from 1.76 to 2.71 W m−2 K−1 on the glass side, the absorber side remaining consistently about 25% higher. These values were applied as boundary conditions in the three-dimensional model.

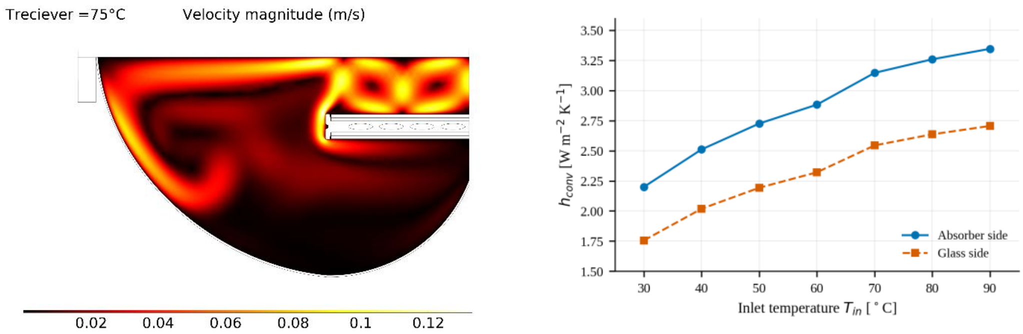

Fig. 6: a) Velocity magnitude of the buoyancy-driven air flow inside the low-concentrating collector cavity, obtained from the two-dimensional CFD model at a receiver temperature of 75 °C. b) Convective heat transfer coefficients inside the low-concentrating receiver cavity obtained from the two-dimensional CFD simulations, for fluid inlet temperatures between 30 °C and 90 °C.

3.3. Flat-plate collector

Fig. 7a compares the thermal efficiency curves of the three modified flat-plate configurations with the validated reference design, and Tab. 3 lists the corresponding parameters. It can be observed that all modified configurations increase the zero-loss efficiency, from 0.486 for the reference case to 0.525 (FP-EXT1, +8.1%), 0.520 (FP-EXT2, +7.1%), and 0.500 (FP-VAC1, +2.9%). At the same time, the heat loss coefficient rises from 19.3 W m−2 K−1 to between 22.3 and 24.3 W m−2 K−1, corresponding to increases of 15.4% (FP-EXT1), 26.1% (FP-EXT2), and 20.6% (FP-VAC1). As a result, the modified efficiency curves are steeper and cross the reference curve at reduced temperatures between approximately 0.004 and 0.013 K m² W−1 (Fig. 7a).

Tab. 3: Simulated performance parameters of the flat-plate absorber configurations.

Configuration	Zero-loss efficiency, η_0 [-]	Heat loss coefficient, a_1 [W/(m²·K)]	Pressure loss [Pa]
FP-VAC (reference)	0.486	19.28	299.5
FP-EXT1	0.525	22.26	67.5
FP-EXT2	0.520	24.31	61.3
FP-VAC1	0.500	23.26	213.1

Fig. 7 shows the temperature distribution of the working fluid in the four flat-plate absorbers at an inlet temperature of 25 °C. In the reference design the fluid heats progressively along the flow direction and the outlet region is the warmest part of the absorber, whereas the extrusion-based designs distribute the flow over a larger number of parallel channels, which shortens the thermal entry length and produces a more uniform temperature field across the absorber width. The same subdivision explains the hydraulic result: the many parallel channels of FP-EXT1 and FP-EXT2 carry the same total flow at a lower velocity per channel, which is the direct cause of the reduction in pressure loss reported in Tab. 3.

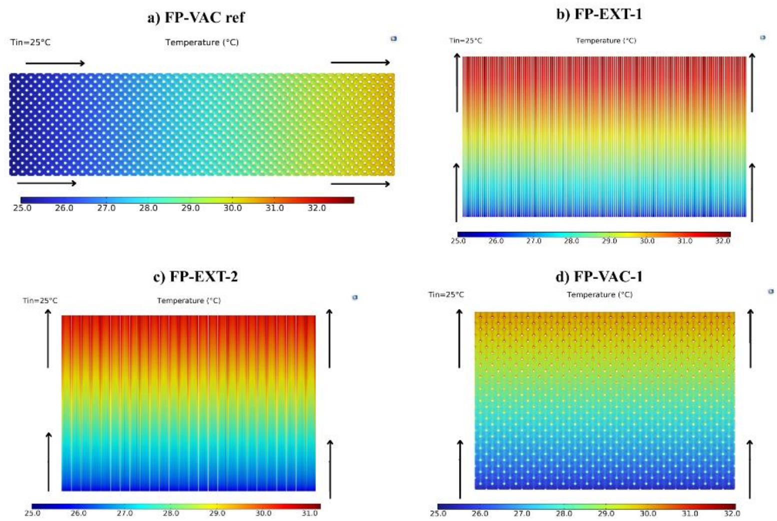

Fig. 7: Simulated temperature distribution of the working fluid in the flat-plate absorbers at an inlet temperature of 25 °C: (a) FP-VAC reference, (b) FP-EXT1, (c) FP-EXT2, (d) FP-VAC1. The temperature range of each panel is given in its label.

For a conventional solar-thermal collector, this combination would be a defect; for a heat pump source it is the intended behavior. When the collector feeds the heat pump evaporator, the mean fluid temperature lies near or below the ambient temperature, so the operating point lies at the far left of Fig. 8a, and frequently at negative reduced temperatures. In this window, a higher zero-loss efficiency and a steeper curve are both advantageous: the absorber extracts more solar heat and, when operating below ambient, gains additional heat from the surrounding air (Bertram et al., 2012). The modified designs therefore outperform the reference across the entire operating range relevant for heat pump integration. The channel redesign simultaneously reduces the pressure loss, by 77.5% for FP-EXT1, 79.5% for FP-EXT2, and 28.9% for FP-VAC1 (Fig. 8b, Tab. 3), which lowers the parasitic pumping power of the collector loop. Taking the three metrics together, FP-EXT2 offers the strongest profile for heat pump integration: a 7.1% gain in zero-loss efficiency, the largest increase in heat loss coefficient (+26.1%), and an 80% reduction in pressure loss.

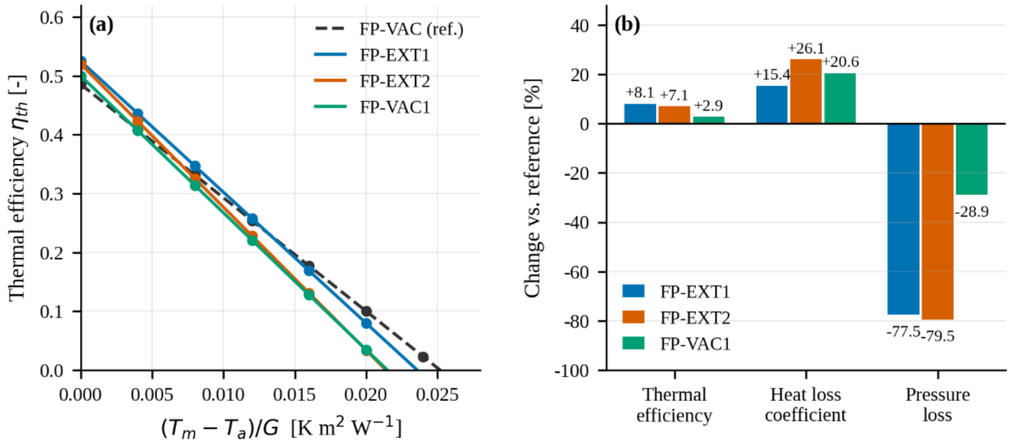

Fig. 8: Simulated performance of the modified flat-plate absorber configurations relative to the reference design: (a) thermal efficiency curves; (b) relative changes in zero-loss thermal efficiency, heat loss coefficient, and pressure loss (positive values denote an increase).

3.4. Low-concentrating collector

The design logic reverses for the low-concentrating collector, which delivers heat at up to 140 °C and therefore operates far above ambient temperature: here, thermal losses must be suppressed rather than exploited. The zero-loss efficiency gains of the modified configurations are moderate, from 0.538 for the reference to 0.558 (LC-EXT1, +3.9%), 0.554 (LC-EXT2, +3.0%), and 0.548 (LC-EXT3, +2.0%) (Tab. 4), but the decisive parameter is the heat loss coefficient. Only LC-EXT3 reduces it, by 5.0% (from 5.12 to 4.87 W m−2 K−1), whereas LC-EXT1 and LC-EXT2 increase it by 7.7% and 4.9%, respectively.

Tab. 4: Simulated performance parameters of the low-concentrating absorber configurations.

Configuration	Zero-loss efficiency, η_0 [-]	Heat loss coefficient, a_1 [W/(m²·K)]	Pressure loss, Δp [Pa]
LC-EXT (reference)	0.538	5.12	223.2
LC-EXT1	0.558	5.52	208.1
LC-EXT2	0.554	5.37	77.4
LC-EXT3	0.548	4.87	492.9

The temperature fields of the four low-concentrating absorbers are compared in Fig. 9 at an inlet temperature of 20 °C. All configurations raise the fluid temperature by a similar amount along the absorber, which is consistent with the modest differences in zero-loss efficiency reported in Tab. 4, but the internal distribution differs: the micro-grooved channels of LC-EXT3 keep the fluid closer to the heated wall over the whole cross-section, which is what reduces the temperature difference driving the losses to the cavity and explains its lower heat loss coefficient.

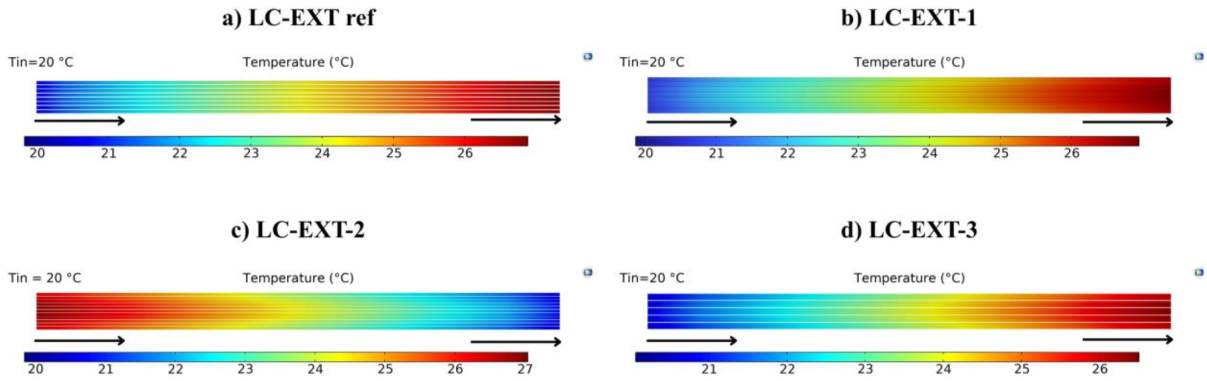

Fig. 9: Simulated temperature distribution of the working fluid in the low-concentrating absorbers at an inlet temperature of 20 °C: (a) LC-EXT reference, (b) LC-EXT1, (c) LC-EXT2, (d) LC-EXT3.

The consequence is visible in Fig. 10a. Although LC-EXT1 shows the largest gain at zero reduced temperature, its higher heat loss coefficient erodes this advantage as the operating temperature increases, and beyond approximately 0.05 K m² W−1 its efficiency falls below the reference. LC-EXT3 shows the opposite behavior: the combination of a modest zero-loss gain with the lowest heat loss coefficient keeps its curve above all other configurations across the operating region relevant for industrial process heat. This thermal advantage carries a hydraulic price: the micro-grooved channels of LC-EXT3 increase the pressure loss by 120.8%, more than doubling the pumping requirement, while LC-EXT2 reduces the pressure loss by 65.4% and LC-EXT1 by 6.8% (Fig. 10b).

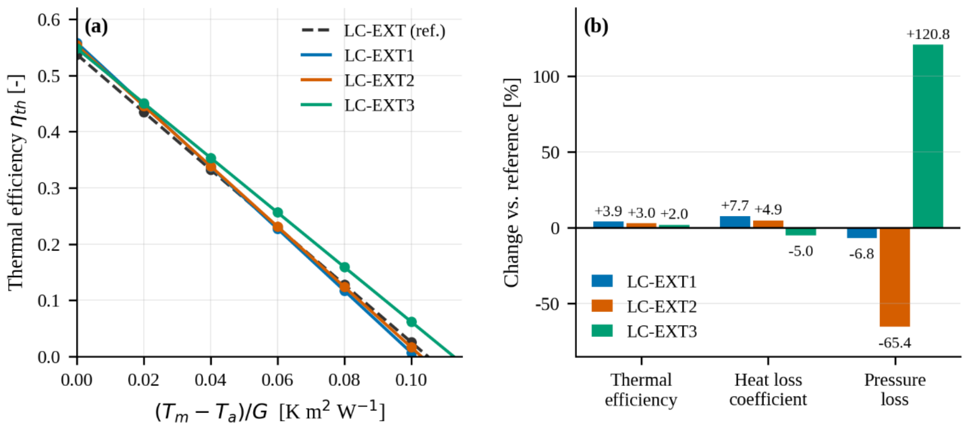

Fig. 10: Simulated performance of the modified low-concentrating absorber configurations relative to the reference design: (a) thermal efficiency curves; (b) relative changes in zero-loss thermal efficiency, heat loss coefficient, and pressure loss (positive values denote an increase).

No single low-concentrating configuration dominates all three metrics. LC-EXT3 maximizes thermal performance at operating temperature but at a substantial hydraulic penalty; LC-EXT2 offers a balanced profile combining a moderate efficiency gain with a strong pressure-loss reduction; LC-EXT1 is attractive only near ambient conditions. The appropriate choice therefore depends on whether the intended process is limited by thermal losses at high delivery temperature or by the available pumping power, which is a system-level rather than a collector-level decision.

3.5. Manufacturing cost analysis

Applying the cost model of Section 2.7 to the input parameters of Tab. 2 gives the unitary manufacturing costs and the tooling investments that drive the comparison. For the flat-plate absorber, vacuum forming combines a low tooling investment of 25,000 € with a high unitary cost of 47.38 €/unit, whereas extrusion inverts this profile, requiring 129,091 € of tooling but only 32.87 €/unit. For the polymer variant of the low-concentrating absorber the same tooling investments apply, while the smaller absorber area of 0.45 m² lowers the unitary costs to 23.23 €/unit for vacuum forming and 16.21 €/unit for extrusion. The resulting cost curves are shown in Fig. 11. For the flat-plate absorber they intersect at approximately 7,200 units: below this volume vacuum forming remains the more economical route, above it extrusion is preferable. For the low-concentrating absorber the smaller area reduces the per-unit saving of extrusion and shifts the break-even to approximately 14,800 units.

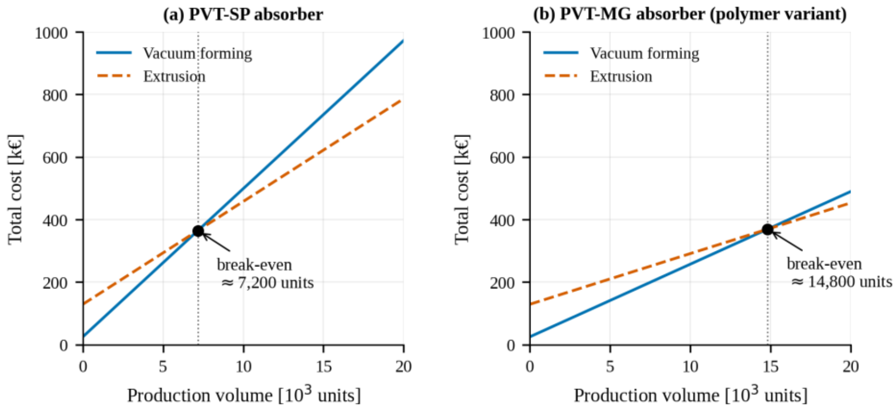

Fig. 11: Total manufacturing cost of the (a) flat-plate and (b) low-concentrating PVT absorbers produced by vacuum forming and extrusion as a function of production volume, with break-even volumes indicated.

These thresholds connect the manufacturing analysis directly to the performance results. The two best-performing flat-plate designs, FP-EXT1 and FP-EXT2, are extrusion-based and are therefore economically rational only at production volumes above roughly 7,200 units; below this volume, the vacuum-formed FP-VAC1 remains the appropriate choice despite its smaller performance gains. For the low-concentrating collector, all investigated channel geometries assume extrusion, so the threshold of approximately 14,800 units marks the volume above which the polymer absorber variant becomes viable. Absorber selection is consequently not a pure performance optimization but a joint performance–manufacturing decision governed by the expected production volume.

4. Conclusion

This study investigated the role of thermal absorber design in flat-plate and low-concentrating PVT collectors using a CFD model-based assessment combined with a simplified manufacturability analysis. The results demonstrate that absorber geometry optimization has a strong impact on thermal performance and hydraulic behavior, with application-specific trade-offs observed between heat extraction, heat loss, and pressure loss. For flat-plate PVT collectors targeting heat pump integration, designs with higher heat loss coefficients and improved zero loss thermal efficiency were found to be advantageous, while for low-concentrating PVT systems, absorber design primarily influenced thermal loss reduction and hydraulic penalties. The manufacturing analysis shows that the two production routes are separated by a break-even volume of approximately 7,200 units for the flat-plate absorber and 14,800 units for the low-concentrating absorber: below these volumes vacuum forming is the cheaper route, above them extrusion is. The available manufacturing process and the expected production volume therefore act as design constraints on the absorber geometry itself, since the channel shapes that can be produced, and the volume at which they become affordable, differ between the two routes. The reference designs investigated in this work are experimentally validated within the PVT4EU project. Future work will include experimental results, an extended assessment of the influence of absorber design on electrical efficiency, and an enhanced techno-economic analysis incorporating payback time and environmental impact for journal publication.

5. Acknowledgement

This work has been developed under the framework of PVT4EU project, granted by the Clean Energy Transition Partnership Programme (project ID. CETP 2022-00403). The work is supported by national funds through, Sweden: Swedish Energy Agency (P2023-00884); Denmark: Innovation Fund Denmark (3112-00010B); and Portugal: FCT- Fundação para a Ciência e a Tecnologia, I.P. (CETP/0004/2022).

6. References

Armstrong, S., Hurley, W.G., 2010. A thermal model for photovoltaic panels under varying atmospheric conditions. Applied Thermal Engineering 30, 1488–1495. https://doi.org/10.1016/j.applthermaleng.2010.03.012

Beltrán, F., Sommerfeldt, N., Eskola, J., Madani, H., 2024. Empirical investigation of solar photovoltaic-thermal collectors for heat pump integration. Applied Thermal Engineering 248, 123175. https://doi.org/10.1016/j.applthermaleng.2024.123175

Beltrán, F., Sommerfeldt, N., Reichl, C., Madani, H., 2025. Cold solar: PVT heat exchanger designs for heat pump integration. Applied Thermal Engineering 261, 125020. https://doi.org/10.1016/j.applthermaleng.2024.125020

Bertram, E., Glembin, J., Rockendorf, G., 2012. Unglazed PVT collectors as additional heat source in heat pump systems with borehole heat exchanger. Energy Procedia 30, 414–423. https://doi.org/10.1016/j.egypro.2012.11.049

Herrando, M., Wang, K., Huang, G., Otanicar, T., Bany Mousa, O., Agathokleous, R.A., Ding, Y., Kalogirou, S., Ekins-Daukes, N., Taylor, R.A., Markides, C.N., 2023. A review of solar hybrid photovoltaic-thermal (PV-T) collectors and systems. Progress in Energy and Combustion Science 97, 101072. https://doi.org/10.1016/j.pecs.2023.101072

Hollands, K.G.T., Unny, T.E., Raithby, G.D., Konicek, L., 1976. Free convective heat transfer across inclined air layers. Journal of Heat Transfer 98, 189–193. https://doi.org/10.1115/1.3450517

Kurniawati, I., Sung, Y., 2024. A review of heat dissipation and absorption technologies for enhancing performance in photovoltaic–thermal systems. Energies 17, 1721. https://doi.org/10.3390/en17071721

Lämmle, M., Oliva, A., Hermann, M., Kramer, K., Kramer, W., 2017. PVT collector technologies in solar thermal systems: A systematic assessment of electrical and thermal yields with the novel characteristic temperature approach. Solar Energy 155, 867–879. https://doi.org/10.1016/j.solener.2017.07.015

Olivares, A., Rekstad, J., Meir, M., Kahlen, S., Wallner, G., 2008. A test procedure for extruded polymeric solar thermal absorbers. Solar Energy Materials and Solar Cells 92, 445–452. https://doi.org/10.1016/j.solmat.2007.10.006

Pranesh, V., Velraj, R., Christopher, S., Kumaresan, V., 2019. A 50 year review of basic and applied research in compound parabolic concentrating solar thermal collector for domestic and industrial applications. Solar Energy 187, 293–340. https://doi.org/10.1016/j.solener.2019.04.056

PVT4EU, 2026. PVT4EU project – next generation photovoltaic-thermal collectors. https://pvt4eu.eu (accessed 14 July 2026).

Ramezani, A.M., Jadidi, A.M., Rashidi, S., 2024. Techno-economic and environmental investigation between a low-concentrating photovoltaic thermal collector and a regular photovoltaic flat plate thermal collector. International Communications in Heat and Mass Transfer 155, 107529. https://doi.org/10.1016/j.icheatmasstransfer.2024.107529

NETZSCH Analyzing & Testing (n.d.) ABS: acrylonitrile-butadiene-styrene copolymer. Available at: https://analyzing-testing.netzsch.com/en/polymers-netzsch-com/commodity-thermoplastics/abs-acrylonitrile-butadiene-styrene-copolymer (Accessed: 27 August 2026).

Herrando, M., Ramos, A., Zabalza, I., & Markides, C. N. (2019). A comprehensive assessment of alternative absorber-exchanger designs for hybrid PVT-water collectors. *Applied Energy, 235*, 1583–1602. https://doi.org/10.1016/j.apenergy.2018.11.024